

# Berry curvature induced thermopower in type-I and type-II Weyl Semimetals

Kamal Das<sup>1,\*</sup> and Amit Agarwal<sup>1,†</sup>

<sup>1</sup>*Dept. of Physics, Indian Institute of Technology Kanpur, Kanpur 208016, India*

Berry curvature acts analogous to a magnetic field in the momentum-space, and it modifies the flow of charge carriers and entropy. This induces several intriguing magnetoelectric and magnetothermal transport phenomena in Weyl semimetals. Here, we explore the impact of the Berry curvature and orbital magnetization on the thermopower in tilted type-I and type-II Weyl semimetals, using semi-classical Boltzmann transport formalism. We analytically calculate the full magnetoconductivity matrix and use it to obtain the thermopower matrix for different orientations of the magnetic field. We find that the tilt of the Weyl nodes induces linear magnetic field ( $B$ ) terms in the conductivity matrix, as well as in the thermopower matrix. The linear- $B$  term appears in the Seebeck coefficients, when the  $B$ -field is applied along the tilt axis. Applying the magnetic field in a plane perpendicular to the tilt axis results in a quadratic- $B$  planar Nernst effect, linear- $B$  out-of-plane Nernst effect and quadratic- $B$  correction in the Seebeck coefficient.

## I. INTRODUCTION

Weyl semimetals (WSMs) host relativistic massless fermionic quasi-particles in vicinity of the Weyl nodes which always come in pairs of opposite chirality<sup>1–4</sup>. Their existence has been demonstrated in several materials<sup>5–9</sup> where either time reversal or space inversion symmetry or both are broken. Unlike their relativistic counterparts, in crystalline systems the Weyl quasiparticles can also break Lorentz invariance. Consequently, their dispersion can be tilted in a specific direction<sup>10–18</sup>. Depending on the degree of the tilt, these WSMs can be classified as type-I or type-II WSM. In a type-I WSM, the Fermi surface encloses only one kind of carriers, and have a vanishing density of states at the Weyl point. In contrast, a type-II WSM has non-vanishing density of states at the Weyl point, and the Weyl point appears at the intersection of an electron and a hole pocket.

Interestingly, the Weyl nodes act as a source or sink of Berry curvature (BC), which in turn act as a fictitious magnetic field in the momentum space<sup>19,20</sup>. This leads to the possibility of several interesting transport phenomena in isotropic and tilted WSMs<sup>21–35</sup>. Several of these have also been experimentally demonstrated<sup>5,7,35–48</sup>. For instance, negative magnetoresistivity (MR)<sup>21,24</sup> has been observed in several WSM candidates including the TaAs family<sup>37,38,44</sup> and in WSMs induced magnetically from three dimensional Dirac semimetals<sup>5,7,40</sup>. The anomalous Hall effect<sup>49</sup> predicted to exist in time reversal symmetry (TRS) broken WSMs<sup>34,50</sup> has been recently seen in ZrTe<sub>5</sub><sup>45</sup>. The corresponding effect in thermopower, the anomalous Nernst effect in WSM<sup>29,33</sup> has been demonstrated in Cd<sub>3</sub>As<sub>2</sub><sup>42</sup>, NbP<sup>35</sup> and Ti<sub>2</sub>MnX<sup>47</sup>. Chiral magnetic effect, a chiral anomaly induced phenomena<sup>22,23,30</sup> has been reported in ZrTe<sub>5</sub><sup>51</sup>. The BC induced planar Hall effect, where the current response is measured in the plane of electric and magnetic field, has also been predicted in WSM<sup>52,53</sup> and multi-WSM<sup>54,55</sup> and experimentally demonstrated in WSM<sup>46,48</sup>. More recently, linear magnetic field dependence in both the MR and Hall responses is predicted to exist in tilted WSMs<sup>56–58</sup>.

Motivated by these recent studies, in this paper we explore the BC induced magnetothermopower in tilted type-I and type-II WSMs: the Seebeck and the Nernst coefficients (SCs and NCs, respectively). Our analytical calculations for the full conductivity and thermopower matrix, are based on the Berry-connected-Boltzmann-transport formalism and include the effect of the orbital magnetic moment (OMM)<sup>20</sup>. The Seebeck effect captures the electric response along the temperature gradient while the Nernst effect captures electric response perpendicular to the temperature gradient. The conductivity and the thermopower are connected by the Mott relation [see Eq. (4)] even in the presence of OMM correction<sup>59</sup>. Thus the magnetothermopower broadly follows the magnetoelectric response, leading to the expectation of phenomena like negative Seebeck effect and planar Nernst effects in WSMs. Similar kind of phenomena is known to exist in ferromagnetic systems<sup>60,61</sup> where spin dependent scattering induces a transverse velocity component in the charge carriers<sup>62</sup>.

Our analytical calculation for the full conductivity and thermopower matrix focuses on impact of tilt, BC and OMM on the anisotropic magnetotransport in type-I and type-II WSM. In particular this paper highlights the following BC induced phenomena: (1) negative longitudinal (parallel electric and magnetic field) magnetoresistance (MR) and positive perpendicular (perpendicular electric and magnetic field) MR in WSM, (2) linear- $B$  as well as quadratic- $B$  dependent SCs, (3) the existence of quadratic- $B$  planar Nernst as well as linear- $B$  out-of-plane Nernst response. The paper is organized as follows: Section II survey of the Boltzmann transport theory of thermopower in presence of the BC. This is followed by a detailed discussion of the full magnetoconductivity matrix for type-I and type-II WSM in Sec. III, and MR in Sec. IV. This is followed by a discussion of the full thermopower matrix in Sec. V. Finally we summarize our findings in Sec. VI.

## II. THERMOPOWER IN PRESENCE OF BERRY CURVATURE

Within the linear response theory, the phenomenological transport equation for the charge current  $\mathbf{j}^e$  is given by<sup>63</sup>,

$$j_i^e = \sigma_{ij} E_j + \alpha_{ij} (-\nabla_j T). \quad (1)$$

Here  $E_j$  and  $\nabla_j T$  are the external electric field and temperature gradient applied along the  $j$ th direction,  $\sigma_{ij}$  denotes the elements of electrical conductivity matrix ( $\tilde{\sigma}$ ) and  $\alpha_{ij}$  are the elements of thermoelectric conductivity matrix ( $\tilde{\alpha}$ ). The transport coefficients such as  $\sigma_{ij}$  and  $\alpha_{ij}$  are calculated by doing a Brillouin zone sum over the relevant physical quantities, involving only the occupied states. In this paper, we use the semiclassical Boltzmann transport formalism to calculate the magnetoconductivity and magnetothermopower. The details of the Berry-connected-Boltzmann-transport formalism is discussed in appendix A. The general expressions for BC induced conductivity and thermopower are presented in Eq. (A10), and (A11), respectively.

The thermopower for an open circuit system is defined by setting  $j_i^e = 0$  in Eq. (1). In this scenario, the electric field generated by a temperature gradient is given by,

$$E_i = \nu_{ij} \nabla_j T, \text{ where } \tilde{\nu} \equiv \tilde{\sigma}^{-1} \tilde{\alpha}. \quad (2)$$

The diagonal elements  $\nu_{ii}$  denote the SCs whereas the off-diagonal elements  $\nu_{ij} (i \neq j)$  are the NCs. It turns out that in the low temperature limit ( $k_B T \ll \mu$ ), BC induced thermopower can also be expressed in terms of the conductivity using the Mott relation<sup>59</sup>. The Mott relation<sup>63,64</sup> yields,

$$\alpha_{ij} = -\frac{\pi^2 k_B^2 T}{3e} \left. \frac{\partial \sigma_{ij}}{\partial \epsilon} \right|_{\epsilon=\mu}. \quad (3)$$

Using Eq. (3) in Eq. (2), the thermopower matrix can be expressed solely in terms of the conductivity matrix as<sup>63,64</sup>

$$\tilde{\nu} = -\frac{\pi^2 k_B^2 T}{3e} \tilde{\sigma}^{-1} \left. \frac{\partial \tilde{\sigma}}{\partial \epsilon} \right|_{\epsilon=\mu}. \quad (4)$$

Further, to explicitly track the magnetic field dependence analytically, we express  $\sigma_{ij} = \sigma_{ij}^{(0)} + \sigma_{ij}^{(1)} + \sigma_{ij}^{(2)} + \mathcal{O}(B^3)$ , and  $\alpha_{ij} = \alpha_{ij}^{(0)} + \alpha_{ij}^{(1)} + \alpha_{ij}^{(2)} + \mathcal{O}(B^3)$ . Here the superscripts denotes zeroth order (Drude and anomalous), linear and quadratic magnetic field terms, respectively. In the next section, we calculate the magnetoconductivity matrix for tilted WSM, including the OMM corrections. Since the tilt-axis (say  $\hat{\mathbf{R}}$ ) breaks the TRS for each node, the two cases of when  $\mathbf{B}$  is applied parallel and perpendicular to  $\hat{\mathbf{R}}$  result in different forms of the conductivity matrix.

## III. MAGNETOCONDUCTIVITY IN TYPE-I AND TYPE-II WSM

The low energy Hamiltonian, for each of the chiral node of a tilted WSM is given by,<sup>65</sup>

$$\mathcal{H}_s(\mathbf{k}) = \hbar C_s k_z + s \hbar v_F \boldsymbol{\sigma} \cdot \mathbf{k}. \quad (5)$$

Here,  $s$  denotes chirality,  $C_s$  ( $v_F$ ) is the tilt (Fermi) velocity and  $\boldsymbol{\sigma} = (\sigma_x, \sigma_y, \sigma_z)$ , are the Pauli spin matrices. In this paper, we consider a WSM with a pair of oppositely tilted node such that  $C_{-s} = -C_s$ . The degree of the tilt of the Weyl nodes can be quantified by the ratio of the tilt and the Fermi velocities:  $R_s = C_s/v_F$ . The above dispersion corresponds to type-I class of WSM in the regime  $|R_s| < 1$  and type-II class in the regime  $|R_s| > 1$ .

The BC can be easily calculated from Eq. (A3) to be  $\boldsymbol{\Omega}_s^\lambda = -\lambda s \mathbf{k}/(2k^3)$ , where  $\lambda = +1$  ( $\lambda = -1$ ) denotes the conduction (valence) band. The OMM can be calculated from Eq. (A4) and can be expressed in terms of the BC<sup>66</sup>,

$$\mathbf{m}_s^\lambda = \lambda e v_F k \boldsymbol{\Omega}_s^\lambda = -s e v_F \frac{\mathbf{k}}{k^2}. \quad (6)$$

Both of the BC and the OMM are independent of the tilt velocity. Furthermore, the OMM, and the resulting velocity correction is identical for both the bands. We define the velocity correction due to OMM as  $\mathbf{v}_\mathbf{k}^m = \frac{1}{\hbar} \nabla_\mathbf{k}(\mathbf{m}_\mathbf{k} \cdot \mathbf{B})$ .

The impact of the tilt on the magnetoconductivity in type-I and type-II WSM was explored in Ref. [58]. Here we generalize those results to include the effect of OMM. The conductivity matrix can be expressed as sum of contributions in absence and presence of a magnetic field:  $\tilde{\sigma} = \tilde{\sigma}_D + \tilde{\sigma}_B$ , such that  $\tilde{\sigma}_B$  vanishes as  $\mathbf{B} \rightarrow 0$  and  $\tilde{\sigma}_D$  is the Drude conductivity. For the scenario in which  $\mathbf{B} \perp \hat{\mathbf{R}}$ , and the magnetic field is confined in the  $x$ - $y$  plane (planar geometry), we find that the conductivity matrix has this general form for both type-I and type-II WSMs,

$$\tilde{\sigma}_B = \begin{pmatrix} \sigma_\perp^{(2)} + \Delta\sigma^{(2)} \cos^2 \phi & \Delta\sigma^{(2)} \sin(2\phi)/2 & \sigma_t^{(1)} \cos \phi \\ \Delta\sigma^{(2)} \sin(2\phi)/2 & \sigma_\perp^{(2)} + \Delta\sigma^{(2)} \sin^2 \phi & \sigma_t^{(1)} \sin \phi \\ \sigma_t^{(1)} \cos \phi & \sigma_t^{(1)} \sin \phi & \sigma_z^{(2)} \end{pmatrix}. \quad (7)$$

Here,  $\phi$  is the angle of the magnetic field with respect to the  $x$  axis. See appendix (B) for the details of calculation of the Drude conductivity ( $\tilde{\sigma}_D$ ). Here  $\sigma_{12} = \sigma_{xy}$  denotes the planar Hall conductivity and in addition there are new linear- $B$  terms such as  $\sigma_{13} = \sigma_{zx}$  and  $\sigma_{23} = \sigma_{yz}$ , which were discussed in Ref. [58].

For the other case of  $\mathbf{B} \parallel \hat{\mathbf{R}}$ , the general form of the conductivity matrix has a diagonal form<sup>58</sup>,

$$\tilde{\sigma}_B = \begin{pmatrix} \sigma_1^{(2)} + \sigma_1^{(1)} & 0 & 0 \\ 0 & \sigma_1^{(2)} + \sigma_1^{(1)} & 0 \\ 0 & 0 & \sigma_{1z}^{(1)} + \sigma_{1z}^{(2)} \end{pmatrix}. \quad (8)$$

Here, the diagonal conductivity terms also have linear- $B$  terms induced by the tilt of the Weyl nodes. The analytical expression of the different conductivity components, is presented in the subsections below.

### A. Type-I WSMs

For the  $\mathbf{B} \perp \mathbf{R}$  case, the magnetoconductivity is given by Eq. (7), where the conductivity coefficients  $\sigma_{\perp}^{(2)}$ ,  $\sigma_z^{(2)}$  and  $\Delta\sigma^{(2)}$  are proportional to  $B^2$ . In a type-I WSM, these are explicitly given by

$$\sigma_{\perp}^{(2)} = \sum_s (1 - 3\gamma) \sigma_0, \quad (9)$$

$$\Delta\sigma^{(2)} = \sum_s [7 + 13R_s^2 - \gamma(1 + 6R_s^2)] \sigma_0, \quad (10)$$

$$\sigma_z^{(2)} = \sum_s [1 + 7R_s^2 - \gamma(3 - R_s^2)] \sigma_0. \quad (11)$$

Here, the factor  $\gamma = 1$  (0) explicitly keeps track of the terms arising from the presence (absence) of the OMM<sup>67</sup>, and we have defined

$$\sigma_0 \equiv \frac{e^2 \tau}{8\pi^2} \frac{\hbar v_F^3}{15\mu^2} \left( \frac{eB}{\hbar} \right)^2. \quad (12)$$

These terms are finite even in the limit of  $R_s \rightarrow 0$  and are even function of  $R_s$ . Thus, the contributions from a pair of oppositely tilted nodes just adds up. Furthermore, the corrections due to OMM (the  $\gamma$  dependent terms) tend to suppress the conductivities. Note that the inclusion of OMM in the conductivity changes the sign of  $\sigma_{\perp}^{(2)}$ . This will manifest in the perpendicular MR (in  $\sigma_{xx}$  for  $\phi = \pi/2$ ) being positive, and the longitudinal MR (in  $\sigma_{xx}$  for  $\phi = 0$ ) being negative, as discussed in the next section.

In addition to these quadratic- $B$  terms, there are linear- $B$  dependent off-diagonal conductivity components as well ( $\sigma_{xz}, \sigma_{yz} \propto \sigma_t^{(1)} \propto B$ ). These terms arise solely due to the tilt of the Weyl nodes (which breaks the TRS for each node), and vanish in the limit of  $R_s \rightarrow 0$ . These linear- $B$  components are  $\sigma_{xz}^{(1)} = \sigma_{yz}^{(1)} (\pi/2 - \phi) = \sigma_t^{(1)} \cos \phi$ , where  $\sigma_t^{(1)}$  can be expressed as

$$\sigma_t^{(1)} = \sum_s \frac{s\sigma_1}{6R_s^4} [2R_s \{ (3 - 2R_s^2)(\gamma - 1) + 3R_s^2(1 - 2R_s^2) \} + 3\mathcal{F}\delta_s(\gamma - 1 + R_s^2)]. \quad (13)$$

In Eq. (13), we have defined  $\mathcal{F} \equiv 1 - R_s^2$  and,

$$\sigma_1 = \frac{e^2 \tau}{(2\pi)^3} \frac{\pi v_F}{\hbar} \frac{eB}{\hbar}, \text{ and } \delta_s = \ln \left( \frac{1 - R_s}{1 + R_s} \right).$$

Note that the contributions for the oppositely tilted nodes simply add up.

For the  $\mathbf{B} \parallel \mathbf{R}$  configuration, the conductivity matrix is given by Eq. (8). As the matrix structure shows, in

this case the longitudinal conductivities have a linear- $B$  term in addition to the quadratic- $B$  term. Quadratic- $B$  correction perpendicular to the tilt is  $\sigma_{\perp}^{(2)} = \sigma_{\perp}^{(2)} = (1 - 3\gamma)\sigma_0$ , whereas along the tilt axis it is given by

$$\sigma_{\text{lz}}^{(2)} = \sum_s [8 + \gamma(5R_s^2 - 4)] \sigma_0. \quad (14)$$

The linear- $B$  term in  $\sigma_{xx} = \sigma_{yy}$  is given by

$$\sigma_1^{(1)} = \sum_s \frac{s\sigma_1}{6R_s^4} [2R_s \{ (3 - 2R_s^2)(\gamma - 1) - 6\gamma R_s^2 \} - 3\delta_s \{ (R_s^2 - 1)(\gamma - 1) + 2\gamma R_s^2 \}]. \quad (15)$$

For  $\sigma_{zz}$ , the linear- $B$  correction is given by

$$\sigma_{\text{lz}}^{(1)} = \sum_s \frac{s\sigma_1}{3R_s^4} [2R_s \{ (3 - 5R_s^2)(1 - \gamma) - 3R_s^4 \} + 3\mathcal{F}^2 \delta_s(1 - \gamma)]. \quad (16)$$

We emphasize that all the linear- $B$  conductivity terms discussed in this section  $\propto \sigma_1$ , in which there is no explicit  $\mu$  dependence. This is primarily a consequence of  $\Omega_{\mathbf{k}} \propto 1/k^2$  in WSMs. The only  $\mu$  dependence of  $\sigma_1$  arises from the energy dependence of the scattering timescale  $\tau$ .

### B. Type-II WSMs

The low energy model Hamiltonian of Eq. (5) corresponds to type-II class in the regime  $|C_s| > v_F$ . In this regime, Fermi surface of the low energy Hamiltonian of the Weyl node comprises of “unbounded” electron and hole pockets. Hence both the bands take part in transport. And to truncate the “unbounded sea” of the charge carriers, we need to introduce a cutoff in the momentum space along the radial direction ( $\Lambda_k$ ). In real materials, this is akin to the bandwidth of the system. For simplicity, we present all the conductivity terms only upto first order in  $k_F/\Lambda_k \equiv 1/\tilde{\Lambda}_k$ , and assume  $\mu > 0$  without the loss of generality.

First, we will consider the planar geometry ( $\mathbf{B} \perp \mathbf{R}$ ). In this case the form of the conductivity matrix is given by Eq. (7), and the elements of the conductivity matrix are given by

$$\Delta\sigma^{(2)} = \sum_s \mathcal{K} (\mathcal{A}_{\mathcal{R}} - \gamma \mathcal{A}_{\mathcal{M}}), \quad (17)$$

$$\sigma_{\perp}^{(2)} = \sum_s \mathcal{K} (\mathcal{B}_{\mathcal{R}} - \gamma \mathcal{B}_{\mathcal{M}}), \quad (18)$$

$$\sigma_z^{(2)} = 2 \sum_s \mathcal{K} (\mathcal{D}_{\mathcal{R}} - \gamma \mathcal{D}_{\mathcal{M}}). \quad (19)$$

where  $\mathcal{K} \equiv \frac{\sigma_0}{16|R_s|^5}$ . For the planar Hall (responses in the  $x$ - $y$  plane) components of the conductivity, we have

defined the following polynomials of  $R_s$ :

$$\mathcal{A}_{\mathcal{R}} = 2(1 - R_s^2 + 5R_s^4 + 125R_s^6 + 30R_s^8), \quad (20)$$

$$\mathcal{A}_{\mathcal{M}} = 2(3 + 8R_s^2 - 45R_s^4 + 90R_s^6), \quad (21)$$

$$\mathcal{B}_{\mathcal{R}} = (1 - 5R_s^2 + 15R_s^4 + 5R_s^6), \quad (22)$$

$$\mathcal{B}_{\mathcal{M}} = 3(1 - 10R_s^2 + 25R_s^4). \quad (23)$$

For the  $\sigma_{zz}$  component, we have defined the following polynomials of  $R_s$ ,

$$\mathcal{D}_{\mathcal{R}} = (-2 + 11R_s^2 - 25R_s^4 + 65R_s^6 + 15R_s^8), \quad (24)$$

$$\mathcal{D}_{\mathcal{M}} = 2(-3 + 6R_s^2 + 5R_s^4). \quad (25)$$

Note that the tilt induced corrections occur as even powers of  $R_s$ , implying addition of contribution from the oppositely tilted nodes. The linear- $B$  correction in the out-of-plane off-diagonal conductivities can be written as  $\sigma_{xz}^{(1)} = \sigma_{yz}^{(1)}(\pi/2 - \phi) = \sigma_t^{(1)} \cos \phi$ . Here,

$$\begin{aligned} \sigma_t^{(1)} = \sum_s \frac{s\sigma_1}{6R_s^4} \text{sgn}(R_s) & \left[ (11 - 24R_s^2 + 21R_s^4)(\gamma - 1) \right. \\ & \left. + 3\gamma(2 + R_s^2 - 5R_s^4) - 3\mathcal{F}\delta_s^1(\gamma - 1 + R_s^2) \right], \quad (26) \end{aligned}$$

and we have defined

$$\delta_s^1 = \ln(R_s^2 - 1) + 2 \ln \tilde{\Lambda}_k. \quad (27)$$

Now, we consider magnetic field along the direction of the tilt ( $\mathbf{B} \parallel \mathbf{R}$ ). The linear- $B$  correction to the longitudinal component in  $x/y$  plane,  $\sigma_{xx} = \sigma_{yy}$ , is given by

$$\begin{aligned} \sigma_1^{(1)} = \sum_s \frac{s\sigma_1}{6R_s^4} \text{sgn}(R_s) & \left[ (11 - 9R_s^2)(\gamma - 1) - 6\gamma(3R_s^2 - 1) \right. \\ & \left. - 3\delta_s^1 \{ (R_s^2 - 1)(1 - \gamma) - 2\gamma R_s^2 \} \right]. \quad (28) \end{aligned}$$

The linear- $B$  correction to  $\sigma_{zz}$  is given by

$$\begin{aligned} \sigma_{1z}^{(1)} = \sum_s \frac{s\sigma_1}{3R_s^4} \text{sgn}(R_s) & \left[ (17 - 27R_s^2 + 6R_s^4)(1 - \gamma) \right. \\ & \left. - 6(1 - 2R_s^2 + 2R_s^4) + 3\delta_s^1 \mathcal{F}^2(\gamma - 1) \right]. \quad (29) \end{aligned}$$

The quadratic- $B$  correction to  $\sigma_{xx}$  and  $\sigma_{yy}$  is given by

$$\sigma_1^{(2)} = \sum_s \frac{\sigma_0}{8|R_s|^5} [(-2 + 5R_s^2 + 5R_s^6) + 6\gamma(1 - 5R_s^2)]. \quad (30)$$

The corresponding term for the  $\sigma_{zz}$  component is given by

$$\sigma_{1z}^{(2)} = \sum_s \frac{\sigma_0}{2|R_s|^5} [(1 - 5R_s^2 + 15R_s^4 + 5R_s^6) \quad (31)$$

$$+ \gamma(-3 + 10R_s^2 - 20R_s^4 + 15R_s^6)]. \quad (32)$$

Having obtained the full conductivity matrix for tilted WSM, we now discuss tilt and OMM dependence of the MR – the quantity generally probed in experiments.

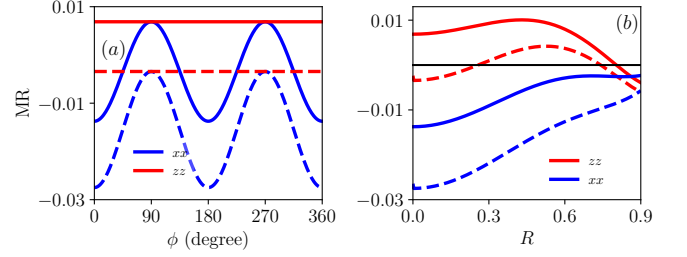


FIG. 1. a) MR for type-I WSM ( $R = 0$ ) as a function of the angle between  $\mathbf{E}$  and  $\mathbf{B}$  for the planar geometry. The planar MR ( $MR_{xx}(\phi)$ ) varies as  $\cos^2 \phi$ . The longitudinal MR is negative irrespective of OMM correction. The perpendicular MR becomes positive on including the OMM (solid red line). (b) However, on varying the degree of tilt ( $R$ ) [ $R_+ = R_- = -R$ ],  $MR_{xx}(\phi = 0)$  remains negative while  $MR_{zz}$  changes sign at a certain critical  $R$  value, beyond which it remains negative. Here, we have used the following parameters:  $\mu = 0.1$  eV,  $\tau = 10^{-12}$  sec,  $v_F = 10^6$  m/s and  $B = 4$  T.

#### IV. MAGNETORESISTIVITY

The resistivity matrix is obtained by inverting the conductivity matrix. The corresponding MR is given by  $MR_{ii} = \rho_{ii}(B)/\rho_{ii}(0) - 1$ . Below we discuss the longitudinal and perpendicular MR for the two cases of  $\mathbf{B} \perp \mathbf{R}$  and  $\mathbf{B} \parallel \mathbf{R}$ .

For the case of  $\mathbf{B} \perp \mathbf{R}$ , using Eq. (7), we obtain the ‘planar’ resistivity to be

$$\rho_{xx} = \rho_D - \rho_{\perp}^{(2)} + \left[ \left( \rho_t^{(1)} \right)^2 \rho_D^z [\rho_D]^{-2} - \Delta \rho^{(2)} \right] \cos^2 \phi. \quad (33)$$

Here, we have defined the Drude resistivity in the  $x$ - $y$  plane as  $\rho_D = 1/\sigma_D$ , and along the  $z$  axis as  $\rho_D^z = 1/\sigma_D^z$ . Additionally, we have defined the following:  $\rho_{\perp}^{(2)} = \sigma_{\perp}^{(2)}/\sigma_D^2$ ,  $\rho_t^{(1)} = \sigma_t^{(1)}/\sigma_D^2$  and  $\Delta \rho^{(2)} = \Delta \sigma^{(2)}/\sigma_D^2$ . The ‘planar’ MR [ $MR_{xx}(\phi)$ ] varies as  $\cos^2 \phi$  on changing the planar  $\mathbf{B}$  direction with respect to the  $x$  axis. The longitudinal MR [ $MR_{xx}(\phi = 0)$ ] is negative irrespective of inclusion or exclusion of the OMM and the degree of the tilt of WSM. The perpendicular MR [ $MR_{xx}(\phi = \pi/2)$ ] becomes positive on including the OMM terms ( $\gamma = 1$ ) for isotropic WSMs. This is highlighted in Fig. 1 (a) which shows the variation of  $MR_{xx}$  as a function of  $\phi$ , for the cases of  $\gamma = 0$  (dashed blue line) and  $\gamma = 1$  (solid blue line). For the out-of-plane transverse MR ( $MR_{zz}$ ), we obtain the resistivity to be

$$\rho_{zz} = \rho_D^z - \rho_z^{(2)} + \left( \rho_{tz}^{(1)} \right)^2 \rho_D [\rho_D^z]^{-2}. \quad (34)$$

Here, we have defined  $\rho_z^{(2)} = \sigma_z^{(2)}/\sigma_D^z$  and correction due to the linear- $B$  Hall conductivity component as  $\rho_{tz}^{(1)} = \sigma_t^{(1)}/\sigma_D^z$ . The OMM correction forces the out-of-plane transverse MR ( $MR_{zz}$ ) to be positive (solid red line) for

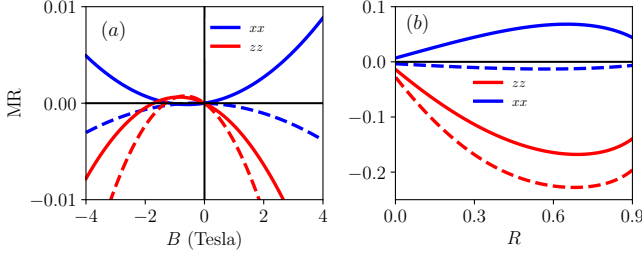


FIG. 2. (a) The magnetic field dependence of the MR for the case of  $\mathbf{B} \parallel \mathbf{R}$  and the tilt configuration of the last figure. Note that  $\text{MR}_{xx}$  and  $\text{MR}_{zz}$  have a linear- $B$  contribution for a finite tilt (here  $R = .015$ ), leading to an asymmetry in the MR curves about the  $B = 0$  line. (b) Variation of MR for type-I WSM as a function of the tilt parameter  $R$ , for the case of  $\mathbf{B} \parallel \mathbf{R}$ . Note that the inclusion of OMM correction forces  $\text{MR}_{xx}$  to be positive in this case (solid blue line), while  $\text{MR}_{zz}$  remains negative with or without OMM correction (solid or dashed red line, respectively). Here the parameters and tilt configuration used are identical to those of Fig. 1.

WSM with small tilt – as shown in panels (a) and (b) of Fig. 1.

For the other case of  $\mathbf{B} \parallel \mathbf{R}$ , we calculate resistivity along the tilt direction from Eq. (8), and it is given by

$$\rho_{zz} = \rho_D^z - \rho_{lz}^{(1)} + \left(\rho_{lz}^{(1)}\right)^2 [\rho_D^z]^{-1} - \rho_{lz}^{(2)}. \quad (35)$$

Here we have defined  $\rho_{lz}^{(1)} = \sigma_{lz}^{(1)}/(\sigma_D^z)^2$  and  $\rho_{lz}^{(2)} = \sigma_{lz}^{(2)}/(\sigma_D^z)^2$ . Evidently, in this case the longitudinal MR,  $\text{MR}_{zz}$ , will have linear- $B$  contribution for a tilted WSM, while its absolute value depends on the degree of the tilt, starting with a negative MR for an isotropic WSM. This linear- $B$  part gives rise to an asymmetry in the MR curve as  $B$  goes from negative to positive – see Fig. 2(a). Note that the inclusion of OMM does not change the sign of longitudinal MR. The corresponding expression for  $\rho_{xx}$  is given by

$$\rho_{xx} = \rho_D - \rho_l^{(1)} + \left(\rho_l^{(1)}\right)^2 [\rho_D]^{-1} - \rho_l^{(2)}. \quad (36)$$

Here, we have defined  $\rho_l^{(1)} = \sigma_l^{(1)}/\sigma_D^2$  and  $\rho_l^{(2)} = \sigma_l^{(2)}/\sigma_D^2$ . Similar to the case of  $\rho_{zz}$ ,  $\rho_{xx}$  also has linear- $B$  contributions leading to asymmetric MR curves around the  $B = 0$  line shown in Fig. 2(a). However, unlike the case of longitudinal MR, the perpendicular MR,  $\text{MR}_{xx}$  changes sign on including the OMM and reverses from negative to positive as shown in Fig. 2(b).

Our findings for isotropic WSM that the longitudinal MR is negative, while the perpendicular MR is positive, is consistent with the experimental MR results reported in Dirac semimetal<sup>7,40</sup> and isotropic WSMs<sup>37,44</sup>. We emphasize that the inclusion of OMM is crucial to capture the correct sign of the perpendicular MR.

## V. THERMOPOWER IN WEYL SEMIMETAL

In this section we calculate the magnetic field dependent thermopower at low temperature using Mott relation<sup>59</sup>. Let us first consider the case  $\mathbf{B} \perp \mathbf{R}$ . Since  $\tilde{\alpha} \propto \partial_\mu \tilde{\sigma}$ , the thermoelectric conductivity matrix retains the form of Eq. (7), and it is given by

$$\tilde{\alpha}_{\mathbf{B}} = \begin{pmatrix} \alpha_{\perp}^{(2)} + \Delta\alpha^{(2)} \cos^2 \phi & \Delta\alpha^{(2)} \sin(2\phi)/2 & \alpha_t^{(1)} \cos \phi \\ \Delta\alpha^{(2)} \sin(2\phi)/2 & \alpha_{\perp}^{(2)} + \Delta\alpha^{(2)} \sin^2 \phi & \alpha_t^{(1)} \sin \phi \\ \alpha_t^{(1)} \cos \phi & \alpha_t^{(1)} \sin \phi & \alpha_z^{(2)} \end{pmatrix}. \quad (37)$$

The different thermoelectric conductivity terms in the matrix are connected to the corresponding terms in the conductivity matrix of Eq. (7) via the Mott relation [Eq. (3)]. At a first glance it seems that the out-of-plane Hall components ( $\alpha_{xz}$  and  $\alpha_{yz} \propto \alpha_t^{(1)}$ ) are zero for type-I WSM as the corresponding terms in the charge conductivity matrix are independent of the Fermi energy. However, the scattering timescale is generally dependent on the Fermi energy, and this would lead to a finite linear- $B$  term in the thermoelectric conductivity matrix as well. Another possibility is that the deviations from the linear model, for example in a lattice model, can also lead to finite linear- $B$  contribution. Similar physics is seen in case of the finite anomalous Nernst response in a tight-binding model of WSMs<sup>29</sup>, even though the anomalous Hall coefficient is independent of the chemical potential in the isotropic low energy model of WSM<sup>27</sup>.

The thermopower matrix can now be calculated by using Eqs. (7) and (37) in Eq. (2). The SC in the planar configuration can be expressed in the form  $\nu_{yy} = \nu_{xx}(\pi/2 - \phi)$ , where

$$\nu_{xx} - \nu_D = \nu_{\perp}^{(2)} + \Delta\nu^{(2)} \cos^2 \phi. \quad (38)$$

Here, we have defined  $\nu_D = \alpha_D/\sigma_D$  as the usual Drude coefficient calculated in appendix (B) and the magnetic field dependent coefficients are given by

$$\begin{aligned} \nu_{\perp}^{(2)} &= \sigma_D^{-2} \left( \sigma_D \alpha_{\perp}^{(2)} - \alpha_D \sigma_{\perp}^{(2)} \right), \\ \Delta\nu^{(2)} &= \frac{1}{\sigma_D^2} \left( \sigma_D \Delta\alpha^{(2)} - \alpha_D \Delta\sigma^{(2)} + \left( \sigma_t^{(1)} \alpha_D - \alpha_t^{(1)} \sigma_D \right) \frac{\sigma_t^{(1)}}{\sigma_D^z} \right). \end{aligned} \quad (39)$$

The out-of-plane SC (along the  $z$  axis) can be expressed as  $\nu_{zz} = \nu_D^z + \nu_z^{(2)}$ , where  $\nu_D^z \equiv \alpha_D^z/\sigma_D^z$  is the Drude contribution along the tilt axis and the corresponding quadratic- $B$  correction is given by

$$\nu_z^{(2)} = \frac{1}{(\sigma_D^z)^2} \left( \sigma_D^z \alpha_z^{(2)} - \alpha_D^z \sigma_z^{(2)} + \left( \sigma_t^{(1)} \alpha_D^z - \alpha_t^{(1)} \sigma_D^z \right) \frac{\sigma_t^{(1)}}{\sigma_D} \right). \quad (40)$$

For the planar configuration, we obtain the coefficient for the planar Nernst effect,

$$\nu_{yx} = \Delta\nu^{(2)} \sin \phi \cos \phi. \quad (41)$$



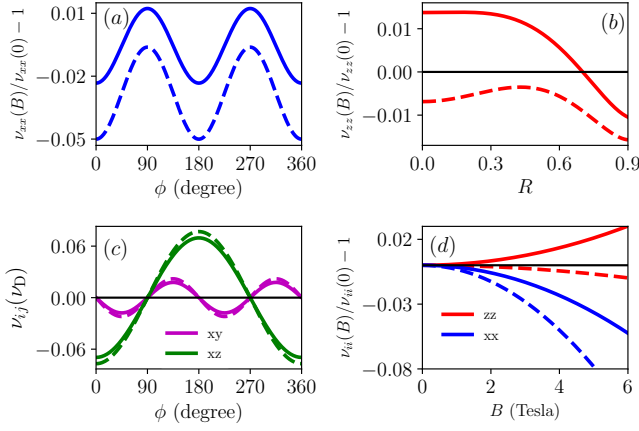


FIG. 3. Various components of thermopower for type-I class with  $R_+ = R_- = -R$  in the planar geometry. (a) The  $\cos^2 \phi$  dependence of the planar SC including (solid line) and excluding (dashed line) the OMM correction. (b) The dependence of the out-of-plane SC with the tilt parameter. Note that the inclusion of OMM correction (solid line) changes the sign of the  $B$  dependent contribution from negative to positive, up to a critical  $R$ . (c) The angular dependence of the planar NC ( $\nu_{xy} \propto \sin 2\phi$ ) and the out-of-plane NC ( $\nu_{xz} \propto \cos \phi$ ). (d) The  $B$  dependence of the longitudinal and the out-of-plane transverse SC, which results in negative and positive Seebeck effect. We have used the parameters of Fig. 1 and  $R = .015$ .

This has an identical angular dependence on the planar angle between  $\mathbf{E}$  and  $\mathbf{B}$  to that of the planar Hall effect. In addition to the planar Nernst effect, we find the out-of-plane linear- $B$  NCs, and are given by  $\nu_{xz} = \nu_t^{(1)} \cos \phi = \nu_{yz}(\pi/2 - \phi)$ , with

$$\nu_t^{(1)} = \frac{1}{\sigma_D^z} \left( \frac{\alpha_t^{(1)} \sigma_D^z - \sigma_t^{(1)} \alpha_D^z}{\sigma_D} \right). \quad (43)$$

The angular dependence of the planar SC ( $\nu_{xx} \propto \cos^2 \phi$ ), the planar NC ( $\nu_{xy} \propto \sin 2\phi$ ) and the out-of-plane NC ( $\nu_{xz} \propto \cos \phi$ ) is highlighted in Fig. 3(a) and (c), and Fig. 4(a) and (c), for type-I and type-II WSM, respectively. Note that for type-I WSM, the out-of-plane NC is negative for  $\phi = 0$ , while it changes sign to become positive for type-II WSM. The inclusion of OMM has significant impact on the SCs. It reverses the sign of the  $B$ -induced contribution in the  $\nu_{zz}$  for type-I WSM from negative to positive upto a critical tilt parameter, beyond which it retains its negative value [see Fig. 3(b)]. This is reminiscent of the sign change also seen in the perpendicular MR in Fig. 1 (b).

In the presence of BC, magnetic field suppresses the longitudinal SC ( $\nu_{xx}(\phi = 0)$ ) resulting in what is termed as negative Seebeck effect. At the same time, it enhances the perpendicular SC ( $\nu_{zz}$ ) for type-I WSM, as shown in Fig. 3(d). This kind of negative longitudinal Seebeck effect and positive perpendicular Seebeck effect has been experimentally observed in the magnetically

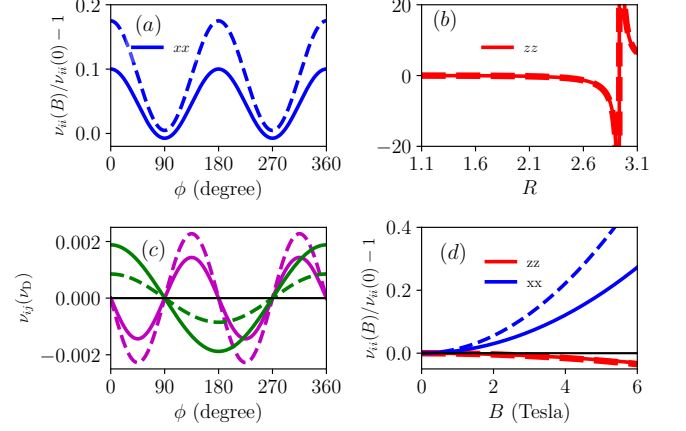


FIG. 4. Same as Fig. 3, but for type-II WSM. (a) The  $\phi$  dependence of  $\nu_{xx}$ . (b) The tilt dependence of  $\nu_{zz}$  has contributions from electrons as well as holes. Here the sign reversal in  $\nu_{zz}$  from negative to positive arises from the sign of the Drude component reversing at large  $R$  (see Fig. 7). This is a direct consequence of the hole carriers dominating the transport on increasing the WSM tilt. (c) The  $\phi$  dependence of planar ( $\nu_{xy}$  - purple curve) and out-of-plane ( $\nu_{xz}$  - green curve) NCs. Note the phase difference of  $\pi$  in the  $\nu_{xz}$  response between type-I and type-II WSM. (d) The  $B$  induced part of the SC has opposite signs for the longitudinal  $\nu_{xx}(\phi = 0)$ , and the out-of-plane transverse  $\nu_{zz}$  components. Here, we have used the parameters of Fig. 1 and the tilt parameter  $R = 1.3$  and cutoff  $\tilde{\Lambda}_k = 10$ .

induced isotropic WSM phase in  $\text{Cd}_3\text{As}_2$ <sup>68</sup> and  $\text{NbP}$ <sup>69</sup>. Our calculations predict that for a type-II WSM, the sign of both the longitudinal and perpendicular SC change as compared to the type-I class, as indicated in Fig. 4(d). However, as a disclaimer we note that this prediction may depend on the specific choice of the cutoff, chemical potential and the tilt parameter.

For the case of the magnetic field along the tilt axis ( $\mathbf{B} \parallel \mathbf{R}$ ), the thermoelectric conductivity matrix can be written as

$$\tilde{\alpha} - \tilde{\alpha}_D = \begin{pmatrix} \alpha_1^{(2)} + \alpha_1^{(1)} & 0 & 0 \\ 0 & \alpha_1^{(2)} + \alpha_1^{(1)} & 0 \\ 0 & 0 & \alpha_{1z}^{(1)} + \alpha_{1z}^{(2)} \end{pmatrix}. \quad (44)$$

Using Eq. (8) and (44) in Eq. (2) yields the thermopower matrix. For this configuration, since both  $\tilde{\sigma}$  and  $\tilde{\alpha}$  are diagonal, the thermopower matrix has no off-diagonal terms *i.e.*, no Nernst response. The diagonal components are given by  $\nu_{xx} = \nu_{yy}$  and

$$\nu_{xx} = \nu_D + \nu_1^{(1)} + \nu_1^{(2)}, \quad (45)$$

$$\nu_{zz} = \nu_D^z + \nu_{1z}^{(1)} + \nu_{1z}^{(2)}. \quad (46)$$

Here we have defined the linear- $B$  correction along  $x$  axis to be

$$\nu_1^{(1)} = \frac{\sigma_D \alpha_1^{(1)} - \alpha_D \sigma_1^{(1)}}{\sigma_D^2}, \quad (47)$$

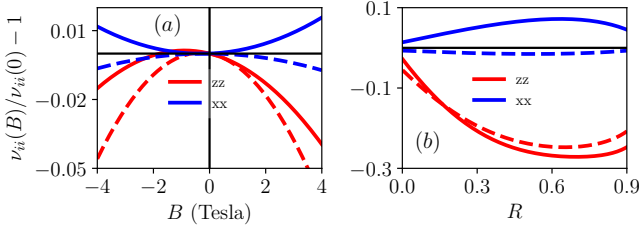


FIG. 5. SCs of type-I class for  $\mathbf{B} \parallel \mathbf{R}$  with  $R_+ = R_- = -R$  tilt configuration. (a) The  $B$  dependence of the SCs at  $R = .015$ . The linear- $B$  terms in the  $\nu_{xx}$  and  $\nu_{zz}$  expressions lead to the asymmetry in the SC curves as  $B$  changes from positive to negative. (b) The tilt dependence of the SCs at  $B = 4$  T. The longitudinal SC ( $\nu_{zz}$ ) is negative irrespective of OMM correction (red lines). Note that the inclusion of the OMM correction has a significant impact on perpendicular SC ( $\nu_{xx}$ ) as evident from the difference between the dashed (excluding OMM) and the solid blue lines (including OMM). We have used all the parameters of Fig 1.

and the quadratic- $B$  correction in Eq. (45) reads as

$$\nu_1^{(2)} = \frac{1}{\sigma_D^2} \left( \alpha_1^{(2)} \sigma_D - \alpha_D \sigma_1^{(2)} + \left( \sigma_1^{(1)} \alpha_D - \alpha_1^{(1)} \sigma_D \right) \frac{\sigma_1^{(1)}}{\sigma_D} \right). \quad (48)$$

The linear and quadratic- $B$  correction along  $z$  direction can be generated from the above two equations simply by replacing the  $x$  component of  $\sigma$ 's and  $\alpha$ 's by their  $z$  components.

Interestingly, the SCs have a linear- $B$  dependence, arising from TRS breaking tilt of each of the Weyl node. This is reminiscent of similar linear- $B$  terms also appearing in the corresponding conductivity matrix. The tilt and  $B$  dependence of the longitudinal SCs for a type-I WSM is shown in Fig. 5, while the same for a type-II WSM is shown in Fig. 6. Evidently the OMM plays an important role, reversing the sign of transverse SC ( $\nu_{xx}$ ) in a type-I as well as type-II WSM. Furthermore, in case of a type-II WSM the linear- $B$  component of  $\nu_{xx}$  dominates for small  $B$ , and the corresponding curve for  $\nu_{xx}(B)/\nu_{xx}(0) - 1$  is almost linear in Fig. 6(a), with a negative slope.

## VI. CONCLUSIONS

The presence of a BC and OMM in WSM influences the flow of charge carriers as well as entropy in presence of magnetic field. This manifests as several interesting magnetoelectric and magnetothermal transport properties in WSM. In this paper, we have focussed on the impact of the BC and OMM on the thermopower of tilted type-I and type-II WSM. Our analytical calculations of the full conductivity and thermopower matrix, are based on the BC-connected semiclassical Boltzmann transport formalism, and explicitly include the effects of the OMM.

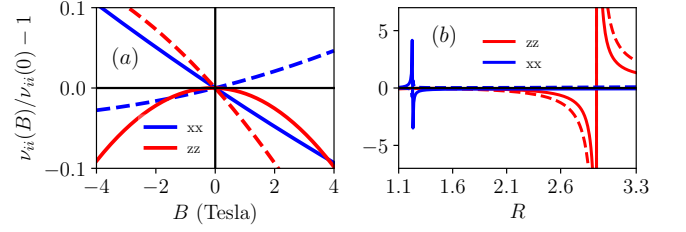


FIG. 6. Same as Fig. 5, but for type-II WSM. (a)  $B$  dependence of the SCs at  $R = 1.3$ . The linear- $B$  terms in  $\nu_{xx}$ , dominates its behaviour for small  $B$  with a negative slope, as shown. (b) The tilt dependence of the SC at  $B = 4$  T. Note that for a given  $R$ , the signs of  $\Delta\nu_{xx}(B)/\nu_{xx}(0)$  and  $\Delta\nu_{zz}(B)/\nu_{zz}(0)$  are opposite. The sign reversal in each of them is a consequence of the corresponding Drude components flipping sign. This in turn occurs as different carriers start dominating the transport as shown in Fig. 7.

The latter modifies the energy-dispersion of the Bloch electrons which also manifests in the modified velocity of carriers, as well as in the Fermi function. However, the Mott relation connecting the conductivity matrix to the thermopower matrix remain intact on including the effects of OMM.

We find that the OMM has a significant impact on the perpendicular MR in WSMs. Consistent with experiments, our calculations show that the longitudinal ( $\mathbf{B} \parallel \mathbf{E}$ ) MR in isotropic WSM is always negative, while the perpendicular MR ( $\mathbf{B} \perp \mathbf{E}$ ) is positive on including the effect of the OMM. However in tilted WSM, the perpendicular MR can also flip sign to become negative for large tilt parameter (see Fig. 1 (b)).

In a type-I WSM, for the case of  $\mathbf{B} \perp \mathbf{R}$ , we find that increasing the magnetic field reduces the longitudinal SC, giving rise to negative Seebeck effect in analogy with negative MR [see Fig. 3(d)]. For the perpendicular SC we find it to be positive for small tilt parameter, but it reverses sign for large tilt parameters. Analogous to the planar Hall effect, we also find the existence of planar Nernst effect, which has an angular dependence  $\nu_{xy} \propto \sin(2\phi)$ . Additionally, we also find a linear- $B$  out-of-plane Nernst response in WSM with a finite tilt. For the other case of  $\mathbf{B} \parallel \mathbf{R}$ , we find the conductivity and the thermopower matrix to be diagonal, with tilt induced linear- $B$  terms in the longitudinal as well as perpendicular components. This manifests in an asymmetry in the MR and SC curve around the  $B = 0$  line, as shown in Figs. 5 and 6.

For the case of a type-II WSM, the scene is a bit mixed up, owing to the contributions of both electron and hole carriers for all energies. We find that even in the absence of a magnetic field, the Drude SC can be positive or negative depending on the tilt (see Fig. 7). For the case of  $\mathbf{B} \perp \mathbf{R}$  in a type-II WSM, we find that in contrast to the case of type-I WSM, the longitudinal SC is positive while the perpendicular SC is negative. The an-

gular dependence of the planar ( $\nu_{xy} \propto \sin 2\phi$ ) and the out-of-plane Nernst effect ( $\nu_{xz} \propto \cos \phi$ ) is the same for type-I and type-II WSM. For the other case of  $\mathbf{B} \parallel \mathbf{R}$ , we find that the linear- $B$  terms dominate the  $\nu_{xx}$  for small magnetic fields. We expect similar effects (such as planar Peltier effect and linear- $B$  out-of-plane Peltier effect among others) to also arise in the diagonal and the off-diagonal coefficients corresponding to the Peltier effect.

### Appendix A: Berry-connected Boltzmann transport formalism

The Boltzmann transport formalism for magnetotransport works well for relatively small magnetic fields where the effects of Landau quantization can be ignored. The equations of motion (EOM) approach work well in the regime where several Landau levels are occupied:  $\hbar\omega_c \ll \mu$ , with  $\mu$  denoting the chemical potential, and  $\omega_c$  is the cyclotron frequency. In addition, the relaxation time approximation for the NDF works well in the regime  $v_F\tau \ll l$ , where  $v_F$  is the Fermi velocity,  $\tau$  is the relaxation time scale and  $l \equiv \sqrt{\hbar/eB}$  is the magnetic length for cyclotron motion<sup>57</sup> with  $B$  as magnetic field.

#### 1. Semiclassical transport with Berry curvature and orbital magnetic moment

The EOM describing the dynamics of the center of the carrier wave-packet (location at  $\mathbf{r}$ , and having the Bloch wave-vector  $\mathbf{k}$ ) in a given band is given by<sup>20,70,71</sup>

$$\dot{\mathbf{r}} = D_{\mathbf{k}} \left( \tilde{\mathbf{v}}_{\mathbf{k}} + \frac{e}{\hbar} (\mathbf{E} \times \boldsymbol{\Omega}_{\mathbf{k}}) + \frac{e}{\hbar} (\tilde{\mathbf{v}}_{\mathbf{k}} \cdot \boldsymbol{\Omega}_{\mathbf{k}}) \mathbf{B} \right), \quad (\text{A1})$$

$$\hbar \dot{\mathbf{k}} = D_{\mathbf{k}} \left( -e\mathbf{E} - e(\tilde{\mathbf{v}}_{\mathbf{k}} \times \mathbf{B}) - \frac{e^2}{\hbar} (\mathbf{E} \cdot \mathbf{B}) \boldsymbol{\Omega}_{\mathbf{k}} \right). \quad (\text{A2})$$

Here  $-e$  is the electronic charge and we have defined  $D_{\mathbf{k}} \equiv [1 + \frac{e}{\hbar} (\mathbf{B} \cdot \boldsymbol{\Omega}_{\mathbf{k}})]^{-1}$ . The band velocity is given by  $\hbar \tilde{\mathbf{v}}_{\mathbf{k}} = \nabla_{\mathbf{k}} \tilde{\epsilon}_{\mathbf{k}}$ , where  $\tilde{\epsilon}_{\mathbf{k}} = \epsilon_{\mathbf{k}} - \mathbf{m}_{\mathbf{k}} \cdot \mathbf{B}$  is the electronic dispersion modified by the intrinsic OMM. The modified band velocity can now be expressed  $\tilde{\mathbf{v}}_{\mathbf{k}} = \mathbf{v}_{\mathbf{k}} - \gamma \mathbf{v}_{\mathbf{k}}^m$ , where  $\mathbf{v}_{\mathbf{k}}^m = \frac{1}{\hbar} \nabla_{\mathbf{k}} (\mathbf{m}_{\mathbf{k}} \cdot \mathbf{B})$ , and the factor of  $\gamma = 0/1$  is introduced to keep track of the OMM dependent corrections.

The BC modified group velocity in Eq. (A1) has two interesting effects: the  $\mathbf{E} \times \boldsymbol{\Omega}_{\mathbf{k}}$  term gives rise to the intrinsic anomalous Hall effect<sup>49,72</sup>, while the  $(\tilde{\mathbf{v}}_{\mathbf{k}} \cdot \boldsymbol{\Omega}_{\mathbf{k}}) \mathbf{B}$  term gives rise to the chiral magnetic effect in presence of non-zero chiral chemical potential<sup>26</sup>. In Eq. (A2), the first two terms are the well known Lorentz force, whereas the third  $(\mathbf{E} \cdot \mathbf{B}) \boldsymbol{\Omega}_{\mathbf{k}}$  term manifests the effect of the chiral anomaly leading to negative MR<sup>24</sup> in WSMs. The modified EOM also changes the phase space volume by a factor  $D_{\mathbf{k}}$ . To compensate for this, such that the number of states in the phase-space volume element is preserved, we have  $d\mathbf{k} \rightarrow d\mathbf{k}/D_{\mathbf{k}}$ . This factor needs to be incorporated whenever the wave-vector summation is converted in an integral over the Brillouin zone in presence of BC<sup>73,74</sup>.

The three component BC and the intrinsic OMM can be obtained from their respective tensors via the relation:  $A_a = \varepsilon_{abc} A^{bc}$ , where  $\varepsilon_{abc}$  is the anti-symmetric Levi-civita symbol. The corresponding Berry tensor is given by<sup>75,76</sup>

$$\boldsymbol{\Omega}_n^{ab} = -2 \frac{\text{Im} [\langle n | \partial_{k_a} \mathcal{H} | n' \rangle \langle n' | \partial_{k_b} \mathcal{H} | n \rangle]}{(\epsilon_n - \epsilon_{n'})^2}, \quad (\text{A3})$$

where  $n$  is the band index with  $\mathcal{H} | n \rangle = \epsilon_n | n \rangle$ . Similarly, the OMM tensor is given by<sup>75,76</sup>

$$\mathbf{m}_n^{ab} = -\frac{e}{\hbar} \frac{\text{Im} [\langle n | \partial_{k_a} \mathcal{H} | n' \rangle \langle n' | \partial_{k_b} \mathcal{H} | n \rangle]}{\epsilon_n - \epsilon_{n'}}. \quad (\text{A4})$$

The dynamics of the NDF  $g_{\mathbf{r},\mathbf{k}}$ , is described by the Boltzmann kinetic equation. In the steady state the NDF kinetic equation for each node is given by<sup>63</sup>

$$\dot{\mathbf{r}} \cdot \nabla_{\mathbf{r}} g_{\mathbf{r},\mathbf{k}} + \dot{\mathbf{k}} \cdot \nabla_{\mathbf{k}} g_{\mathbf{r},\mathbf{k}} = I_{\text{coll}} \{g_{\mathbf{r},\mathbf{k}}\}, \quad (\text{A5})$$

where the right hand side is the collision integral. In the relaxation time approximation,  $I_{\text{coll}} \{g_{\mathbf{r},\mathbf{k}}\} = -\frac{g_{\mathbf{r},\mathbf{k}} - f_{\text{eq}}}{\tau_{\mathbf{k}}}$ , where  $f_{\text{eq}} \equiv f_{\text{eq}}(\tilde{\epsilon}_{\mathbf{k}}, \mu, T) = (e^{\beta(\tilde{\epsilon}_{\mathbf{k}} - \mu)} + 1)^{-1}$  is the equilibrium Fermi-Dirac distribution function with  $\beta^{-1} \equiv k_B T$ . The scattering timescale  $\tau_{\mathbf{k}}$  is the effective intra-node relaxation time which we consider to be constant ( $\tau_{\mathbf{k}} \rightarrow \tau$ ) for simplicity. Substituting Eqs. (A1)-(A2) in Eq. (A5), we obtain an approximate steady state NDF, upto first order in  $\mathbf{E}$  and  $\nabla T$ :

$$g_{\mathbf{r},\mathbf{k}} = f_{\text{eq}} + \left[ D_{\mathbf{k}} \tau \left( -e\mathbf{E} - \frac{(\tilde{\epsilon}_{\mathbf{k}} - \mu)}{T} \nabla_{\mathbf{r}} T \right) \cdot \left( \tilde{\mathbf{v}}_{\mathbf{k}} + \frac{e\mathbf{B}(\tilde{\mathbf{v}}_{\mathbf{k}} \cdot \boldsymbol{\Omega}_{\mathbf{k}})}{\hbar} \right) \right] \left( -\frac{\partial f_{\text{eq}}}{\partial \tilde{\epsilon}_{\mathbf{k}}} \right). \quad (\text{A6})$$

Note that here, we have ignored the terms accounting for the impact of the Lorentz force in modifying the NDF<sup>26,77</sup>. The impact of the Lorentz force is generally small in the low field regime of  $\omega_c \tau \ll 1$  regime<sup>52</sup>. Thus we focus only on the BC induced terms in the rest of the

paper.

Armed with the equation of motion and the NDF, we now proceed to calculate current. In presence of a finite



OMM, the total local current can be expressed as<sup>64</sup>

$$\mathbf{j}^{\text{loc}} = -e \int [d\mathbf{k}] D^{-1} \dot{\mathbf{r}} g_{\mathbf{r},\mathbf{k}} + \nabla_{\mathbf{r}} \times \int [d\mathbf{k}] D^{-1} \mathbf{m}_{\mathbf{k}} f_{\text{eq}}. \quad (\text{A7})$$

Here we have used the shorthand  $[d\mathbf{k}] = d\mathbf{k}/(2\pi)^d$ , with  $d$  being the dimension of the system. The additional second term arises from the intrinsic OMM of individual carriers, and can be physically attributed to the rotating dynamics of the finite width Bloch wave-packet. However, the ‘magnetization current’ is not observable in conventional transport measurement. Consequently, the transport current is defined as<sup>64,78</sup>

$$\mathbf{j}^{\text{tr}} = \mathbf{j}^{\text{loc}} - \nabla_{\mathbf{r}} \times \mathbf{M}(\mathbf{r}), \quad (\text{A8})$$

where  $\mathbf{M}(\mathbf{r})$  is the total orbital magnetization in real space. The magnetization for a given chemical poten-

tial ( $\mu$ ) and  $T$  is given by  $\mathbf{M} = -\partial F / \partial \mathbf{B}|_{\mu, T}$ , where  $F$  is the grand-canonical potential defined as<sup>64</sup>

$$F = -\frac{1}{\beta} \int [d\mathbf{k}] \left( 1 + \frac{e}{\hbar} \mathbf{B} \cdot \boldsymbol{\Omega}_{\mathbf{k}} \right) \ln[1 + e^{-\beta(\tilde{\epsilon}_{\mathbf{k}} - \mu)}]. \quad (\text{A9})$$

Note that in Eq. (A8), the curl in the real space will involve temperature gradients, and the second term gives rise to the anomalous thermo-electric Hall effect.

## 2. Electric and thermoelectric conductivity

Using Eqs. (A1), (A6), and (A9) in Eq. (A8), yields the following general expression for the BC dependent part of the electrical conductivity tensor

$$\sigma_{ij}^{\text{total}} = -\frac{e^2}{\hbar} \int [d\mathbf{k}] \epsilon_{ijl} \Omega_{\mathbf{k}}^l f_{\text{eq}} + e^2 \tau \int [d\mathbf{k}] D_{\mathbf{k}} \left( \tilde{v}_i + \frac{eB_i}{\hbar} (\tilde{\mathbf{v}}_{\mathbf{k}} \cdot \boldsymbol{\Omega}_{\mathbf{k}}) \right) \left( \tilde{v}_j + \frac{eB_j}{\hbar} (\tilde{\mathbf{v}}_{\mathbf{k}} \cdot \boldsymbol{\Omega}_{\mathbf{k}}) \right) \left( -\frac{\partial f_{\text{eq}}}{\partial \tilde{\epsilon}_{\mathbf{k}}} \right). \quad (\text{A10})$$

Here  $\tilde{v}_j$  denotes the  $j$ th component of  $\tilde{\mathbf{v}}_{\mathbf{k}}$ , and  $\epsilon_{ijl}$  is the Levi-Civita antisymmetric tensor. Similarly, the BC dependent part of the thermoelectric conductivity tensor can be explicitly obtained to be

$$\alpha_{ij}^{\text{total}} = \frac{k_B e}{\hbar} \int [d\mathbf{k}] \epsilon_{ijl} \Omega_{\mathbf{k}}^l \xi_{\mathbf{k}} - e\tau \int [d\mathbf{k}] D_{\mathbf{k}} \frac{(\tilde{\epsilon}_{\mathbf{k}} - \mu)}{T} \left( \tilde{v}_i + \frac{eB_i}{\hbar} (\tilde{\mathbf{v}}_{\mathbf{k}} \cdot \boldsymbol{\Omega}_{\mathbf{k}}) \right) \left( \tilde{v}_j + \frac{eB_j}{\hbar} (\tilde{\mathbf{v}}_{\mathbf{k}} \cdot \boldsymbol{\Omega}_{\mathbf{k}}) \right) \left( -\frac{\partial f_{\text{eq}}}{\partial \tilde{\epsilon}_{\mathbf{k}}} \right). \quad (\text{A11})$$

In Eq. (A11) we have defined,

$$\xi_{\mathbf{k}} = \beta(\tilde{\epsilon}_{\mathbf{k}} - \mu) f_{\text{eq}} + \ln[1 + e^{-\beta(\tilde{\epsilon}_{\mathbf{k}} - \mu)}]. \quad (\text{A12})$$

While Eq. (A11) can be evaluated separately, in the low temperature limit ( $k_B T \ll \mu$ ) it can also be obtained from Eq. (A10) by using the Mott relations<sup>63,64</sup> which also hold in the presence of BC and OMM. In fact the validity of Mott relation including the OMM correction has also been proved recently, in a more general setting in Ref. [59].

The first term on the right hand side of Eqs. (A10)-(A11) denote the anomalous Hall effect<sup>49,50,79</sup> and the anomalous thermoelectric effect<sup>27,64</sup>, respectively. In WSM, the anomalous Hall conductivity,  $\sigma_{xy}^A$  has been shown to be linearly proportional to the internode separation<sup>27</sup>. The anomalous thermoelectric conductivity  $\alpha_{xy}^A$  was shown to be zero<sup>27</sup> in linearized model but finite for a lattice model<sup>29,80</sup>. The finite contribution in  $\alpha_{xy}^A$  in a lattice model originates from band curvature

effects beyond the linear dispersion. In case of a tilted WSM, described by a linear dispersion,  $\alpha_{xy}^A$  is finite for both type-I and type-II class of WSM<sup>33</sup>.

In the last term in Eqs. (A10)-(A11), one of the anomalous velocity term arises from the  $\mathbf{E} \cdot \mathbf{B}$  term in Eq. (A2), and the other from the NDF. For parallel electric and magnetic fields, this is what leads to NMR<sup>21,24</sup>, which is quadratic in the magnetic field, and is a relatively well established transport signature<sup>5,37</sup>. This terms also leads to the planar Hall effect<sup>52,53</sup>, in which a Hall voltage is generated in the plane of the electric and magnetic fields, as long as they are not parallel or perpendicular to each other.

Expanding Eqs. (A10)-(A11) in powers of  $B$  (expansion of fermi function<sup>70</sup>), the zeroth order, linear and quadratic- $B$  component of the transport coefficients can be expressed as<sup>63</sup>:  $\sigma_{ij}^{(o)} \equiv \mathcal{L}_{ij}^{0(o)}$  and  $\alpha_{ij}^{(o)} \equiv -\frac{1}{eT} \mathcal{L}_{ij}^{1(o)}$ , where  $o = \{0, 1, 2\}$  refers to the order of magnetic field. For the first order terms we find

$$\begin{aligned} \mathcal{L}_{ij}^{p(1)} = e^2 \tau \int [d\mathbf{k}] & \left[ (\epsilon - \mu)^p \left( \left[ \frac{e}{\hbar} (v_i B_j + v_j B_i) (\mathbf{v} \cdot \boldsymbol{\Omega}) - \frac{e}{\hbar} \boldsymbol{\Omega} \cdot \mathbf{B} v_i v_j \right. \right. \right. \\ & \left. \left. \left. - \gamma (v_i v_j^m + v_j v_i^m) \right] (-f'_0) - \gamma v_i v_j (\mathbf{m} \cdot \mathbf{B}) (-f''_0) \right) - \delta(p-1) (\gamma \mathbf{m} \cdot \mathbf{B})^p v_i v_j (-f'_0) \right]. \end{aligned} \quad (\text{A13})$$

Here  $p = 0$  (or 1) for the electric (or thermoelectric) conductivity. Similarly, the quadratic terms can be expressed as<sup>70</sup>

$$\begin{aligned} \mathcal{L}_{ij}^{p(2)} = e^2 \tau \int [d\mathbf{k}] & \left[ (\epsilon - \mu)^p \left( \left[ v_i v_j \left( \frac{e}{\hbar} \boldsymbol{\Omega} \cdot \mathbf{B} \right)^2 - \frac{e}{\hbar} \boldsymbol{\Omega} \cdot \mathbf{B} \left\{ \frac{e}{\hbar} (v_i B_j + v_j B_i) \mathbf{v} \cdot \boldsymbol{\Omega} - \gamma (v_i v_j^m + v_j v_i^m) \right\} \right. \right. \right. \\ & + \left. \left( \frac{e B_i}{\hbar} \frac{e B_j}{\hbar} (\mathbf{v} \cdot \boldsymbol{\Omega})^2 - \gamma \left\{ \frac{e}{\hbar} (v_i^m B_j + v_j^m B_i) (\mathbf{v} \cdot \boldsymbol{\Omega}) - \frac{e}{\hbar} (v_i B_j + v_j B_i) (\mathbf{v}^m \cdot \boldsymbol{\Omega}) + v_i^m v_j^m \right\} \right) \right] (-f'_0) \\ & - \gamma \left[ \frac{e}{\hbar} (v_i B_j + v_j B_i) (\mathbf{v} \cdot \boldsymbol{\Omega}) - (v_i v_j^m + v_j v_i^m) - v_i v_j \frac{e}{\hbar} \boldsymbol{\Omega} \cdot \mathbf{B} \right] (\mathbf{m} \cdot \mathbf{B}) (-f''_0) + \frac{\gamma}{2} v_i v_j (\mathbf{m} \cdot \mathbf{B})^2 (-f'''_0) \\ & \left. - \delta(p-1) (\gamma \mathbf{m} \cdot \mathbf{B})^p \left[ \left( \frac{e}{\hbar} (v_i B_j + v_j B_i) (\mathbf{v} \cdot \boldsymbol{\Omega}) - (v_i v_j^m + v_j v_i^m) - v_i v_j \frac{e}{\hbar} \boldsymbol{\Omega} \cdot \mathbf{B} \right) (-f'_0) - v_i v_j (\mathbf{m} \cdot \mathbf{B}) (-f''_0) \right] \right]. \end{aligned} \quad (\text{A14})$$

The last term in both Eqs. (A13)-(A14) only contributes to  $\alpha_{ij}$  ( $p = 1$ ). As an additional consistency check, it is straight forward to derive the Mott relations separately for linear- $B$  and quadratic- $B$  terms using Eqs. (A13)-(A14).

## Appendix B: Drude conductivities

In this section we calculate Drude conductivities of tilted WSMs<sup>58,65</sup>. Longitudinal conductivities in absence of magnetic field are called the Drude conductivities. For type-I class, Drude conductivity is given by  $\sigma_{xx}^{(0)} = \sigma_{yy}^{(0)}$ , where

$$\sigma_{xx}^{(0)} = \sum_s \frac{3\sigma_D^0}{4R_s^3} \left[ \frac{2R_s}{(1-R_s^2)} + \ln \left( \frac{1-R_s}{1+R_s} \right) \right]. \quad (\text{B1})$$

Drude conductivity along the  $z$ -direction is given by

$$\sigma_{zz}^{(0)} = \sum_s \frac{3\sigma_D^0}{2R_s^3} \left[ -2R_s - \ln \left( \frac{1-R_s}{1+R_s} \right) \right]. \quad (\text{B2})$$

This is on the account of anisotropy. In the limit  $R_s \rightarrow 0$ , we get Drude conductivity for ideal WSM, which is equal in all three directions and is given by

$$\sigma_D^0 = \frac{4\pi}{3} \frac{e^2}{\hbar} \frac{\mu^2 \tau}{h^2 v_F}. \quad (\text{B3})$$

For type-II class, to calculate the Drude conductivities we need a finite cutoff in momentum space ( $\Lambda_k$ ). Drude conductivity along the  $x$ -direction is given by

$$\sigma_{xx}^{(0)} = \sum_s \frac{3\sigma_D^0}{4|R_s|^3} \left[ \frac{3-R_s^2}{R_s^2-1} + (R_s^2-1) \tilde{\Lambda}_k^2 - \delta_s^1 \right]. \quad (\text{B4})$$

and along the  $z$  direction is given by

$$\sigma_{zz}^{(0)} = \sum_s \frac{3\sigma_D^0}{2|R_s|^3} \left[ 3 - R_s^2 + (R_s^2-1)^2 \tilde{\Lambda}_k^2 + \delta_s^1 \right]. \quad (\text{B5})$$

These expressions of conductivity are exact as there are no approximation due to large cutoff.

Now we discuss the Drude thermopower. The Drude thermopower for isotropic WSM, using Eq. (??) and (B3), calculated to be

$$\nu_D = -\frac{2\pi^2}{3} \frac{k_B}{e} \frac{k_B T}{\mu}. \quad (\text{B6})$$

Note that for a constant relaxation time the Drude Seebeck coefficient is scattering time independent. It is evident that for  $\mu > 0$ , the Drude coefficient is negative and for  $\mu < 0$  it is positive, showing the electron and hole type of carriers respectively. For tilted type-I class, the Drude coefficient is identical to the isotropic. But for type-II class, since the Fermi energy comes along the cut-off, we find considerable effect due to tilt. As in type-II WSMs both the bands contribute and the contributions are opposite in nature, we expect the Drude SC to be zero for equal contribution, which we get in our calculation for large tilt factor limit as shown in fig 7. We have shown the contribution of both the bands. For  $xx$  component valance band dominate in flow of entropy (see fig. 7(a)) whereas for  $zz$  components conduction band dominates (see fig. 7(b)).

## Appendix C: Details of calculation

An alternate way of doing all the calculations, is to use the  $Q \rightarrow 0$  limit along with a spherical geometry with a radial cut-off as done in Ref. [65]. The general expression for conductivity in this case, is given by

$$\begin{aligned} \sigma = \frac{e^2 \tau \mu}{(2\pi)^3} \int_0^\infty k^2 dk \int_0^{2\pi} d\phi_{\mathbf{k}} \int_0^\pi \sin \theta_{\mathbf{k}} d\theta_{\mathbf{k}} & \mathcal{L}(k, \theta_{\mathbf{k}}, \phi_{\mathbf{k}}) \\ & \times \delta(\epsilon_F - \hbar [C_s k \cos \theta_{\mathbf{k}} \pm v_F k]). \end{aligned} \quad (\text{C1})$$

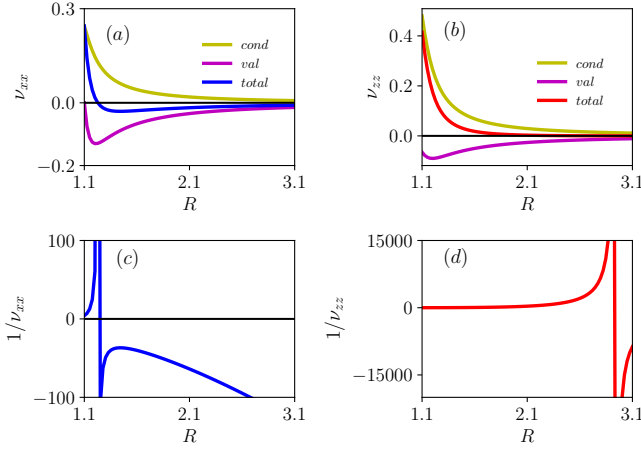


FIG. 7. (a) The Drude ( $B = 0$ ) component of the SC ( $\nu_{xx}$ ), showing the contribution of the conduction and the valance band separately. It reverses sign from positive to negative, as the contribution from the holes (valance band) starts to dominate. (b) The Drude component of the SC ( $\nu_{zz}$ ) highlighting the contribution from the different bands. All the components are scaled by the isotropic Drude counterpart,  $\nu_D$ .

After changing variable,  $\cos \theta_{\mathbf{k}} \rightarrow x$ , it can be rewritten as

$$\sigma = \frac{e^2 \tau_\mu}{(2\pi)^3} \int_0^\infty k^2 dk \int_0^{2\pi} d\phi_{\mathbf{k}} \int_{-1}^1 dx \mathcal{L}(k, x, \phi_{\mathbf{k}}) \times \delta(\epsilon_F - \hbar[C_s k x \pm v_F k]) . \quad (\text{C2})$$

As usual, to solve this integration we use roots of the Dirac delta function. In this case the roots for the conduction band can be calculated to be

$$k_r = \frac{k_F}{R_s x + 1} . \quad (\text{C3})$$

For the positivity of  $k_r$  we must have  $(R_s x + 1) > 0$ . Similarly, for the valance band it is given by

$$k_r = \frac{k_F}{R_s x - 1} , \quad (\text{C4})$$

along with the condition that  $(R_s x - 1) > 0$ . It can be easily checked that for type-I WSMs,  $x$  varies over its entire range  $-1$  to  $1$  (Remember the Fermi energy has to be negative for valence band contribution), while it is not so for the case of type-II WSMs.

For a type-II WSM,  $x = -1/R_s$  sets the limit of  $k$  to infinity. To remedy this situation we introduce a finite momentum cutoff  $\Lambda_k$  to find the limit of  $x$ . For the conduction band with  $R_s > 1$ , we obtain the integration limit to be

$$\left( \frac{k_F}{\Lambda_k} - 1 \right) \frac{1}{R_s} \leq x \leq 1 , \quad (\text{C5})$$

with  $\Lambda_k(R_s + 1) > k_F$  to make the upper limit bigger than the lower limit of  $k$ . Note that for a negative limit of  $x$  the cutoff has to be bigger than  $k_F$ . The lowest limit of  $\Lambda_k$  is determined by the condition  $\Lambda_k > k_F/2$ . Since our results is approximated upto  $k_F/\Lambda_k$ , so we consider  $\Lambda_k \gg k_F$ . When  $R_s < -1$ , we get

$$-1 \leq x \leq \left( \frac{k_F}{\Lambda_k} - 1 \right) \frac{1}{R_s} , \quad (\text{C6})$$

with  $\Lambda_k(1 - R_s) > k_F$ . In the limit  $\Lambda_k \gg k_F$  the higher limit of  $x$  becomes more and more positive. Similarly, for the valance band with positive Fermi energy we derive the following limit:

$$\left( \frac{k_F}{\Lambda_k} + 1 \right) \frac{1}{R_s} \leq x \leq 1 , \quad (\text{C7})$$

with  $\Lambda_k(R_s - 1) > k_F$  for  $R_s > 1$ . Note that the lower limit is also positive. This is due to the fact that we have considered  $\epsilon_F > 0$ . For  $R_s < -1$  we get the following limit

$$-1 \leq x \leq \left( \frac{k_F}{\Lambda_k} + 1 \right) \frac{1}{R_s} , \quad (\text{C8})$$

with  $-\Lambda_k(R_s + 1) > k_F$ . Here also the upper limit is negative. These limits are essential for performing all the integrals for calculating the conductivities.

\* kamaldas@iitk.ac.in

† amitag@iitk.com

<sup>1</sup> H. Nielsen and M. Ninomiya, *Physics Letters B* **105**, 219 (1981)

<sup>2</sup> N. P. Armitage, E. J. Mele, and A. Vishwanath, *Rev. Mod. Phys.* **90**, 015001 (2018)

<sup>3</sup> A. Bansil, H. Lin, and T. Das, *Rev. Mod. Phys.* **88**, 021004

(2016)

<sup>4</sup> B. Yan and C. Felser, *Annual Review of Condensed Matter Physics* **8**, 337 (2017)

<sup>5</sup> H.-J. Kim, K.-S. Kim, J.-F. Wang, M. Sasaki, N. Satoh, A. Ohnishi, M. Kitaura, M. Yang, and L. Li, *Phys. Rev. Lett.* **111**, 246603 (2013)

<sup>6</sup> S.-Y. Xu, I. Belopolski, N. Alidoust, M. Neupane, G. Bian,

- C. Zhang, R. Sankar, G. Chang, Z. Yuan, C.-C. Lee, S.-M. Huang, H. Zheng, J. Ma, D. S. Sanchez, B. Wang, A. Bansil, F. Chou, P. P. Shibayev, H. Lin, S. Jia, and M. Z. Hasan, *Science* **349**, 613 (2015)
- <sup>7</sup> J. Xiong, S. K. Kushwaha, T. Liang, J. W. Krizan, M. Hirschberger, W. Wang, R. J. Cava, and N. P. Ong, *Science* **350**, 413 (2015)
- <sup>8</sup> B. Q. Lv, H. M. Weng, B. B. Fu, X. P. Wang, H. Miao, J. Ma, P. Richard, X. C. Huang, L. X. Zhao, G. F. Chen, Z. Fang, X. Dai, T. Qian, and H. Ding, *Phys. Rev. X* **5**, 031013 (2015)
- <sup>9</sup> S.-Y. Xu, N. Alidoust, I. Belopolski, Z. Yuan, G. Bian, T.-R. Chang, H. Zheng, V. N. Strocov, D. S. Sanchez, G. Chang, C. Zhang, D. Mou, Y. Wu, L. Huang, C.-C. Lee, S.-M. Huang, B. Wang, A. Bansil, H.-T. Jeng, T. Neupert, A. Kaminski, H. Lin, S. Jia, and M. Zahid Hasan, *Nature Physics* **11**, 748 (2015)
- <sup>10</sup> A. A. Soluyanov, D. Gresch, Z. Wang, Q. Wu, M. Troyer, X. Dai, and B. A. Bernevig, *Nature* **527**, 495 (2015)
- <sup>11</sup> G. Autès, D. Gresch, M. Troyer, A. A. Soluyanov, and O. V. Yazyev, *Phys. Rev. Lett.* **117**, 066402 (2016)
- <sup>12</sup> T.-R. Chang, S.-Y. Xu, G. Chang, C.-C. Lee, S.-M. Huang, B. Wang, G. Bian, H. Zheng, D. S. Sanchez, I. Belopolski, N. Alidoust, M. Neupane, A. Bansil, H.-T. Jeng, H. Lin, and M. Zahid Hasan, *Nature Communications* **7**, 10639 (2016)
- <sup>13</sup> P. Li, Y. Wen, X. He, Q. Zhang, C. Xia, Z.-M. Yu, S. A. Yang, Z. Zhu, H. N. Alshareef, and X.-X. Zhang, *Nature Communications* **8**, 2150 (2017)
- <sup>14</sup> J. Jiang, Z. K. Liu, Y. Sun, H. F. Yang, C. R. Rajamathi, Y. P. Qi, L. X. Yang, C. Chen, H. Peng, C.-C. Hwang, S. Z. Sun, S.-K. Mo, I. Vobornik, J. Fujii, S. S. P. Parkin, C. Felser, B. H. Yan, and Y. L. Chen, *Nature Communications* **8**, 13973 (2017)
- <sup>15</sup> S.-Y. Xu, N. Alidoust, G. Chang, H. Lu, B. Singh, I. Belopolski, D. S. Sanchez, X. Zhang, G. Bian, H. Zheng, M.-A. Hsuanu, Y. Bian, S.-M. Huang, C.-H. Hsu, T.-R. Chang, H.-T. Jeng, A. Bansil, T. Neupert, V. N. Strocov, H. Lin, S. Jia, and M. Z. Hasan, *Science Advances* **3**, 1603266 (2017)
- <sup>16</sup> A. Pal, M. Chinotti, L. Degiorgi, W. Ren, and C. Petrovic, *Physica B: Condensed Matter* **536**, 64 (2018)
- <sup>17</sup> M. Zhang, Z. Yang, and G. Wang, *The Journal of Physical Chemistry C* **122**, 3533 (2018)
- <sup>18</sup> G. Chang, B. Singh, S.-Y. Xu, G. Bian, S.-M. Huang, C.-H. Hsu, I. Belopolski, N. Alidoust, D. S. Sanchez, H. Zheng, H. Lu, X. Zhang, Y. Bian, T.-R. Chang, H.-T. Jeng, A. Bansil, H. Hsu, S. Jia, T. Neupert, H. Lin, and M. Z. Hasan, *Phys. Rev. B* **97**, 041104 (2018)
- <sup>19</sup> M. V. Berry, *Proceedings of the Royal Society of London. Series A, Mathematical and Physical Sciences* **392**, 45 (1984)
- <sup>20</sup> D. Xiao, M.-C. Chang, and Q. Niu, *Rev. Mod. Phys.* **82**, 1959 (2010)
- <sup>21</sup> H. Nielsen and M. Ninomiya, *Physics Letters B* **130**, 389 (1983)
- <sup>22</sup> D. T. Son and N. Yamamoto, *Phys. Rev. Lett.* **109**, 181602 (2012)
- <sup>23</sup> A. A. Zyuzin and A. A. Burkov, *Phys. Rev. B* **86**, 115133 (2012)
- <sup>24</sup> D. T. Son and B. Z. Spivak, *Phys. Rev. B* **88**, 104412 (2013)
- <sup>25</sup> P. Hosur and X. Qi, *Comptes Rendus Physique* **14**, 857 (2013)
- <sup>26</sup> K.-S. Kim, H.-J. Kim, and M. Sasaki, *Phys. Rev. B* **89**, 195137 (2014)
- <sup>27</sup> R. Lundgren, P. Laurell, and G. A. Fiete, *Phys. Rev. B* **90**, 165115 (2014)
- <sup>28</sup> A. A. Zyuzin and R. P. Tiwari, *JETP Letters* **103**, 717 (2016)
- <sup>29</sup> G. Sharma, P. Goswami, and S. Tewari, *Phys. Rev. B* **93**, 035116 (2016)
- <sup>30</sup> E. C. I. van der Wurff and H. T. C. Stoof, *Phys. Rev. B* **96**, 121116 (2017)
- <sup>31</sup> T. M. McCormick, R. C. McKay, and N. Trivedi, *Phys. Rev. B* **96**, 235116 (2017)
- <sup>32</sup> A. Sekine, D. Culcer, and A. H. MacDonald, *Phys. Rev. B* **96**, 235134 (2017)
- <sup>33</sup> Y. Ferreiros, A. A. Zyuzin, and J. H. Bardarson, *Phys. Rev. B* **96**, 115202 (2017)
- <sup>34</sup> J. F. Steiner, A. V. Andreev, and D. A. Pesin, *Phys. Rev. Lett.* **119**, 036601 (2017)
- <sup>35</sup> S. J. Watzman, T. M. McCormick, C. Shekhar, S.-C. Wu, Y. Sun, A. Prakash, C. Felser, N. Trivedi, and J. P. Heremans, *Phys. Rev. B* **97**, 161404 (2018)
- <sup>36</sup> W. Desrat, C. Consejo, F. Teppe, S. Contreras, M. Marcinkiewicz, W. Knap, A. Nateprov, and E. Arushanov, *Journal of Physics: Conference Series* **647**, 012064 (2015)
- <sup>37</sup> X. Huang, L. Zhao, Y. Long, P. Wang, D. Chen, Z. Yang, H. Liang, M. Xue, H. Weng, Z. Fang, X. Dai, and G. Chen, *Phys. Rev. X* **5**, 031023 (2015)
- <sup>38</sup> J. Hu, J. Y. Liu, D. Graf, S. M. A. Radmanesh, D. J. Adams, A. Chuang, Y. Wang, I. Chiorescu, J. Wei, L. Spinu, and Z. Q. Mao, *Scientific Reports* **6**, 18674 (2016)
- <sup>39</sup> F. Arnold, C. Shekhar, S.-C. Wu, Y. Sun, R. D. dos Reis, N. Kumar, M. Naumann, M. O. Ajeesh, M. Schmidt, A. G. Grushin, J. H. Bardarson, M. Baenitz, D. Sokolov, H. Bormann, M. Nicklas, C. Felser, E. Hassinger, and B. Yan, *Nature Communications* **7**, 11615 (2016)
- <sup>40</sup> H. Li, H. He, H.-Z. Lu, H. Zhang, H. Liu, R. Ma, Z. Fan, S.-Q. Shen, and J. Wang, *Nature Communications* **7**, 10301 (2016)
- <sup>41</sup> Y. Li, Z. Wang, P. Li, X. Yang, Z. Shen, F. Sheng, X. Li, Y. Lu, Y. Zheng, and Z.-A. Xu, *Frontiers of Physics* **12**, 127205 (2017)
- <sup>42</sup> T. Liang, J. Lin, Q. Gibson, T. Gao, M. Hirschberger, M. Liu, R. J. Cava, and N. P. Ong, *Phys. Rev. Lett.* **118**, 136601 (2017)
- <sup>43</sup> Sudesh, P. Kumar, P. Neha, T. Das, and S. Patnaik, *Scientific Reports* **7**, 46062 (2017)
- <sup>44</sup> A. C. Niemann, J. Gooth, S.-C. Wu, S. Bäßler, P. Sergelius, R. Hühne, B. Rellinghaus, C. Shekhar, V. Süß, M. Schmidt, C. Felser, B. Yan, and K. Nielsch, *Scientific Reports* **7**, 43394 (2017)
- <sup>45</sup> T. Liang, J. Lin, Q. Gibson, S. Kushwaha, M. Liu, W. Wang, H. Xiong, J. A. Sobota, M. Hashimoto, P. S. Kirchmann, Z.-X. Shen, R. J. Cava, and N. P. Ong, *Nature Physics* **14**, 451 (2018)
- <sup>46</sup> N. Kumar, S. N. Guin, C. Felser, and C. Shekhar, *Phys. Rev. B* **98**, 041103 (2018)
- <sup>47</sup> J. Noky, J. Gayles, C. Felser, and Y. Sun, *Phys. Rev. B* **97**, 220405 (2018)
- <sup>48</sup> J. Yang, W. L. Zhen, D. D. Liang, Y. J. Wang, X. Yan, S. R. Weng, J. R. Wang, W. Tong, L. Pi, W. K. Zhu, and C. J. Zhang, *Phys. Rev. Materials* **3**, 014201 (2019)
- <sup>49</sup> F. D. M. Haldane, *Phys. Rev. Lett.* **93**, 206602 (2004)
- <sup>50</sup> A. A. Burkov, *Phys. Rev. Lett.* **113**, 187202 (2014)

- <sup>51</sup> Q. Li, D. E. Kharzeev, C. Zhang, Y. Huang, I. Pletikoscic, A. . V. Fedorov, R. . D. Zhong, J. . A. Schneeloch, G. . D. Gu, and T. Valla, *Nature Physics* **12**, 550 EP (2016)
- <sup>52</sup> S. Nandy, G. Sharma, A. Taraphder, and S. Tewari, *Phys. Rev. Lett.* **119**, 176804 (2017)
- <sup>53</sup> A. A. Burkov, *Phys. Rev. B* **96**, 041110 (2017)
- <sup>54</sup> R. M. A. Dantas, F. Peña-Benitez, B. Roy, and P. Surówka, *Journal of High Energy Physics* **2018**, 69 (2018)
- <sup>55</sup> T. Nag and S. Nandy, arXiv e-prints , arXiv:1812.08322 (2018), [arXiv:1812.08322](#)
- <sup>56</sup> V. A. Zyuzin, *Phys. Rev. B* **95**, 245128 (2017)
- <sup>57</sup> G. Sharma, P. Goswami, and S. Tewari, *Phys. Rev. B* **96**, 045112 (2017)
- <sup>58</sup> K. Das and A. Agarwal, *Phys. Rev. B* **99**, 085405 (2019)
- <sup>59</sup> L. Dong, C. Xiao, and Q. Niu, arXiv e-prints , arXiv:1812.11721 (2018), [arXiv:1812.11721](#)
- <sup>60</sup> C. T. Bui and F. Rivadulla, *Phys. Rev. B* **90**, 100403 (2014)
- <sup>61</sup> C. T. Bui, C. A. C. Garcia, N. T. Tu, M. Tanaka, and P. N. Hai, *Journal of Applied Physics* **123**, 175102 (2018)
- <sup>62</sup> D. Wesenberg, A. Hojem, R. K. Bennet, and B. L. Zink, *Journal of Physics D: Applied Physics* **51**, 244005 (2018)
- <sup>63</sup> N. Ashcroft and N. Mermin, *Solid State Physics*, HRW international editions (Holt, Rinehart and Winston, 1976)
- <sup>64</sup> D. Xiao, Y. Yao, Z. Fang, and Q. Niu, *Phys. Rev. Lett.* **97**, 026603 (2006)
- <sup>65</sup> J. P. Carbotte, *Phys. Rev. B* **94**, 165111 (2016)
- <sup>66</sup> T. Hayata, Y. Kikuchi, and Y. Tanizaki, *Phys. Rev. B* **96**, 085112 (2017)
- <sup>67</sup> F. M. D. Pellegrino, M. I. Katsnelson, and M. Polini, *Phys. Rev. B* **92**, 201407 (2015)
- <sup>68</sup> Z. Jia, C. Li, X. Li, J. Shi, Z. Liao, D. Yu, and X. Wu, *Nature Communications* **7**, 13013 EP (2016)
- <sup>69</sup> U. Stockert, R. D. dos Reis, M. O. Ajeesh, S. J. Watzman, M. Schmidt, C. Shekhar, J. P. Heremans, C. Felser, M. Baenitz, and M. Nicklas, *Journal of Physics: Condensed Matter* **29**, 325701 (2017)
- <sup>70</sup> T. Morimoto, S. Zhong, J. Orenstein, and J. E. Moore, *Phys. Rev. B* **94**, 245121 (2016)
- <sup>71</sup> M. Marder, *Condensed matter physics* (Wiley, Hoboken, N.J, 2010)
- <sup>72</sup> N. A. Sinitsyn, *Journal of Physics: Condensed Matter* **20**, 023201 (2008)
- <sup>73</sup> D. Xiao, J. Shi, and Q. Niu, *Phys. Rev. Lett.* **95**, 137204 (2005)
- <sup>74</sup> C. Duval, Z. Horvath, P. A. Horvathy, L. Martina, and P. C. Stichel, *Modern Physics Letters B* **20**, 373 (2006)
- <sup>75</sup> M.-C. Chang and Q. Niu, *Phys. Rev. B* **53**, 7010 (1996)
- <sup>76</sup> X. Dai, Z. Z. Du, and H.-Z. Lu, *Phys. Rev. Lett.* **119**, 166601 (2017)
- <sup>77</sup> C. Jacoboni, *Theory of electron transport in semiconductors : a pathway from elementary physics to nonequilibrium green functions* (Springer, Berlin, 2010)
- <sup>78</sup> N. R. Cooper, B. I. Halperin, and I. M. Ruzin, *Phys. Rev. B* **55**, 2344 (1997)
- <sup>79</sup> P. Goswami and S. Tewari, *Phys. Rev. B* **88**, 245107 (2013)
- <sup>80</sup> E. V. Gorbar, V. A. Miransky, I. A. Shovkovy, and P. O. Sukhachov, *Phys. Rev. B* **96**, 155138 (2017)